JACS
JOURNAL OF THE AMERICAN CHEMICAL SOCIETY
Communication
pubs.acs.org/JACS

Chemical Unit Cosubstitution and Tuning of Photoluminescence in the $Ca_2(Al_{1-x}Mg_x)(Al_{1-x}Si_{1+x})O_7:Eu^{2+}$ Phosphor

Zhiguo Xia,[*,†,∥] Chonggeng Ma,[*,‡] Maxim S. Molokeev,[§,⊥] Quanlin Liu,[†] Karl Rickert,[∥] and Kenneth R. Poeppelmeier[*,∥]

[†]School of Materials Sciences and Engineering, University of Science and Technology Beijing, Beijing 100083, China
[‡]College of Sciences, Chongqing University of Posts and Telecommunications, Chongqing 400065, China
[§]Laboratory of Crystal Physics, Kirensky Institute of Physics, Siberian Branch of the Russian Academy of Sciences, Krasnoyarsk 660036, Russia
[⊥]Department of Physics, Far Eastern State Transport University, Khabarovsk, 680021, Russia
[∥]Department of Chemistry, Northwestern University, Evanston, Illinois 60208-3113, United States

Supporting Information

ABSTRACT: The union of structural and spectroscopic modeling can accelerate the discovery and improvement of phosphor materials if guided by an appropriate principle. Herein, we describe the concept of "chemical unit cosubstitution" as one such potential design scheme. We corroborate this strategy experimentally and computationally by applying it to the $Ca_2(Al_{1-x}Mg_x)(Al_{1-x}Si_{1+x})O_7:Eu^{2+}$ solid solution phosphor. The cosubstitution is shown to be restricted to tetrahedral sites, which enables the tuning of luminescent properties. The emission peaks shift from 513 to 538 nm with a decreasing Stokes shift, which has been simulated by a crystal-field model. The correlation between the 5d crystal-field splitting of Eu^{2+} ions and the local geometry structure of the substituted sites is also revealed. Moreover, an energy decrease of the electron−phonon coupling effect is explained on the basis of the configurational coordinate model.

Phosphor materials are important in solid-state lighting, flat panel displays, sensors, and biomarkers.[1,2] Given the wide range of technology that employs these materials, new phosphors are highly desirable and are sought after through several strategies, including cationic/anionic substitutions,[3] combinatorial chemistry screenings via phase diagrams,[4] and the newly reported single-particle-diagnosis approach.[5] We propose to expand this list to include the "chemical unit cosubstitution" concept, which has been successfully employed in finding new solid-state materials such as $K_2Al_2B_2O_7$ (nonlinear optic crystal) from $Sr_2Be_2B_2O_7$, $Cu_2ZnSn(S,Se)_4$ (photovoltaic material) from $Cu(In,Ga)Se_2$, and $Zn_xIn_{2-2x}Sn_xO_3$ (transparent conductor) from In_2O_3.[6−8] This design principle is based on the definition and replacement of structural units where the overall sum of the oxidation state of the new unit is the same, but each component is not necessarily isovalent. This methodology has a predilection toward solid solutions, which can be used to discover new phases and/or tune the properties of existing materials.

In the present study, the chemical unit cosubstitution strategy is applied to the melilite structure class $[A_2B(T_2O_7)]$ and the solid solution phosphors, $Ca_2(Al_{1-x}Mg_x)(Al_{1-x}Si_{1+x})O_7:Eu^{2+}$ (x = 0−1), between gehlenite $[Ca_2Al(AlSiO_7)]$ and akermanite $[Ca_2Mg(Si_2O_7)]$.[9−11] This structure family consists of pairs of fused tetrahedra in bow-tie form linked together into sheets by the B cations and separated by the A cations. Scheme 1 depicts the proposed chemical unit cosubstitution of $[Mg^{2+}-Si^{4+}]$ for $[Al^{3+}-Al^{3+}]$, where the cosubstitution is restricted to tetrahedral sites. A combined approach of powder X-ray diffraction (PXRD), solid-state NMR, and first-principles calculations is used to verify this scheme (see the Supporting Information [SI] for experimental and computational details).

Scheme 1. Chemical Unit Cosubstitution of the (a) Melilite-Type $Ca_2(Al_{1-x}Mg_x)(Al_{1-x}Si_{1+x})O_7$ from (b) $Ca_2Al_2SiO_7$ (x = 0) to (f) $Ca_2Mg(Si_2O_7)$ (x = 1) via the Cosubstitution of $[Mg^{2+}-Si^{4+}]$ for $[Al^{3+}-Al^{3+}]$

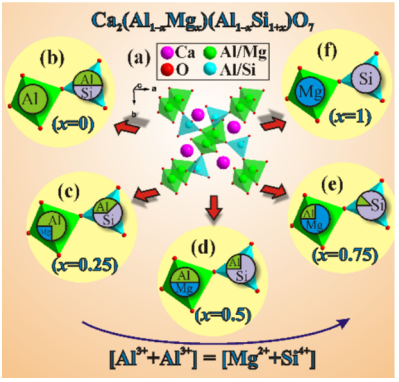

The lattice parameters from Rietveld refinements (Figures S2−S6 and Tables S1 and S2 in the SI) using TOPAS 4.2 and from first-principles calculations are displayed in Figure 1 and demonstrate a high degree of agreement. The lattice parameters and cell volumes show a linear dependence on x, as can be anticipated from Vegard's law.[12] Moreover, the cosubstitution is accompanied by an increase of V and a, but a decrease of c. The

Received: August 13, 2015
Published: September 21, 2015

DOI: 10.1021/jacs.5b08315
J. Am. Chem. Soc. 2015, 137, 12494−12497

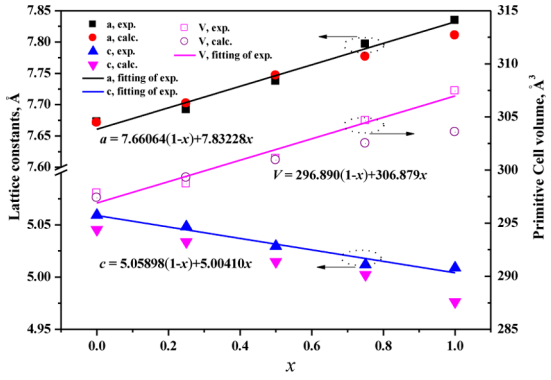

Figure 1. Dependence of the calculated and measured lattice constants (a and c) and primitive cell volume (V) on x of the compounds $Ca_2(Al_{1-x}Mg_x)(Al_{1-x}Si_{1+x})O_7$ (x = 0, 0.25, 0.5, 0.75, and 1).

corresponding equations of the cell parameters as a function of chemical composition, x, are presented in Figure 1 and can be explained by the difference in ionic radii between the substituted and substituting ions. Since the sum of the radii of Mg^{2+} and Si^{4+} is more than double the radius of Al^{3+} and the chemical unit cosubstitution replaces $[Al^{3+}–Al^{3+}]$ with $[Mg^{2+}–Si^{4+}]$, an increasing x leads to the expansion of the cell.[13]

^{29}Si NMR spectra of $Ca_2(Al_{1-x}Mg_x)(Al_{1-x}Si_{1+x})O_7$ for all x show the main peak at ∼−72.3 ppm (Figure S7), which demonstrates that all Si ions in the crystal structure have the same coordination number, CN = 4. Furthermore, using relationships between the δ shift and the Si−O bond lengths in silicates (δ = 999[d_{Si-O}] − 1709), one can compute that, for $Ca_2MgSi_2O_7$, this shift should be equal to −74.6 ppm, which is close to the observed value (−72.4 ppm).[14] Therefore, the NMR data are in good agreement with the Rietveld refinements, and the main changes in local structures should happen no closer than the second coordination sphere. Moreover, the NMR results show that decreasing x leads to the addition of Al on all Si sites, and this cosubstitution shifts the ^{29}Si peaks toward less negative values.

The structural data of $Ca_2(Al_{1-x}Mg_x)(Al_{1-x}Si_{1+x})O_7$ (x = 0, 0.5 and 1) were optimized in a primitive cell with Z = 2. The calculation module "CONFCNT" provided by CRYSTAL09 was used to explore the number of inequivalent symmetry-related configurations that result from the character of the site occupation disorder in these compounds.[15] Two inequivalent symmetry-related configurations for the studied primitive cell of $Ca_2Al_2SiO_7$ were found, whereas the inequivalent symmetry-related configurations for the two cases of x = 0.5 and 1 are unique, respectively. To model the structure of $Ca_2Al_{1.5}Mg_{0.25}Si_{1.25}O_7$, we constructed a supercell with Z = 4 from the obtained structural data of the primitive cell of $Ca_2Al_2SiO_7$ with the lowest total energy by using the symmetrical supercell transformation matrix (1 −1 0; 1 1 0; 0 0 1) for the tetragonal crystal system.[16] With this supercell established, a pair of Mg^{2+} and Si^{4+} ions can be introduced to replace a pair of Al^{3+} ions occupying the B and T sites, respectively. A similar scheme was applied to the case of x = 0.75 by using the obtained structural data of the primitive cell of $Ca_2AlMg_{0.5}Si_{1.5}O_7$. All the inequivalent symmetry-related configurations were run, and the structural data with the lowest total energy for each case were recorded (Table S3), which demonstrate that there is a good agreement (relative error <0.3%) between the calculated data from Rietveld analysis and experimental structural data. Although a systematic slight underestimation can be found for all the cases owing to the use of the hybrid density functional, the calculated trends of a, c, and V on x are fully consistent with the observed ones, as shown in Figure 1.

Photoluminescence excitation (PLE) and photoluminescence emission (PL) spectra for all samples were collected using the relative maxima in emission/excitation intensity found for each sample. The PLE and PL spectra of phosphors $Ca_{1.98}(Al_{1-x}Mg_x)(Al_{1-x}Si_{1+x})O_7$:0.02$Eu^{2+}$ (x = 0, 0.25, 0.5, 0.75, and 1) are depicted in Figure 2a,b. There are two 4f-5d

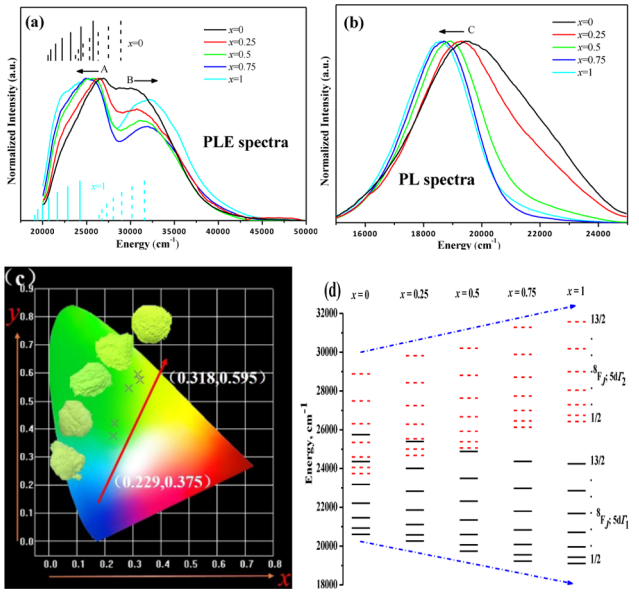

Figure 2. (a) PLE and (b) PL spectra of the phosphors $Ca_{1.98}(Al_{1-x}Mg_x)(Al_{1-x}Si_{1+x})O_7$:0.02$Eu^{2+}$ (x = 0, 0.25, 0.5, 0.75, and 1) as a function of x. The vertical bars represent the calculated 4f-5d zero-phonon transition lines, and their positions and heights show the transition energies and the relative transition line strengths, respectively. (c) CIE chromaticity diagram for the phosphors $Ca_{1.98}(Al_{1-x}Mg_x)(Al_{1-x}Si_{1+x})O_7$:0.02$Eu^{2+}$ (x = 0, 0.25, 0.5, 0.75, and 1) and phosphor images excited at 365 nm. (d) Diagrams for the calculated $4f^6$5d energy levels of Eu^{2+} ions in $Ca_{1.98}(Al_{1-x}Mg_x)$-$(Al_{1-x}Si_{1+x})O_7$:0.02Eu^{2+} (x = 0, 0.25, 0.5, 0.75, and 1).

excitation bands and one 4f-5d emission bands (labeled A, B, and C, respectively, in Figures 2a,b) observed in the PLE and PL spectra for all values of x. The maxima of bands A and C (i.e., E_{ex}(A) and E_{em}(C)) both exhibit a red-shift with increasing x, whereas the maximum of band B (i.e., E_{ex}(B)) exhibits a blue-shift. Thus, it can be concluded that the difference between E_{ex}(A) and E_{ex}(B) increases. Additionally, the emission band C in Figure 2b narrows as x increases from 0 to 1. In other words, the full width at half-maximum (fwhm) of band C exhibits a decreasing trend. The shoulder on the high-energy side of the PL band, between 22 000 and 24 000 cm^{-1}, is due to corrections to the response curve. The shift of band C as a function of x is plotted on the Commission Internationale de L'Eclairage (CIE) chromaticity coordinates in Figure 2c. This reveals that the emission color of this series of phosphors can be tuned from blue-green with color coordinate (0.229, 0.375) to yellow-green (0.318, 0.595) by adjusting the chemical compositions via the $[Mg^{2+}–Si^{4+}]$ unit cosubstitution for $[Al^{3+}–Al^{3+}]$. The observed photoluminescence property data are also in good agreement with the results reported for $Ca_8Mg_3Al_2Si_7O_{28}$:Eu^{2+} by You's group, which is equivalent to x

DOI: 10.1021/jacs.5b08315
J. Am. Chem. Soc. 2015, 137, 12494−12497

= 0.75 in the present study.[17] The detailed values of the spectroscopic parameters mentioned above are listed in Table S4.

The aforementioned shift behaviors of bands A−C in Figure 2a,b induced by the cosubstitution of $[Mg^{2+}-Si^{4+}]$ for $[Al^{3+}-Al^{3+}]$ can be further explained by simple model (SM) analysis.[18] Following this model, bands A and B observed in the 4f-5d PLE spectra can be assigned as the transitions from the $4f^7$ multiplet $^8S_{7/2}$ to the $4f^65d$ states $|(4f^67F,s_d)^8F;5d\Gamma_i\rangle$ (i = 1 and 2), respectively, where s_d represents the 5d spin quantum number and Γ_i is the irreducible representation of the site symmetry group C_s for the ith 5d crystal field (CF) component. It is deduced that $E_{ex}(B) - E_{ex}(A)$ is the energy difference between the lowest two 5d CF components. The band state $|(4f^67F,s_d)^8F;5d\Gamma_i\rangle$ can be further split into seven sub-states $|(4f^67F,s_d)^8F_J;5d\Gamma_i\rangle$ (J = 1/2, ..., 13/2) by the 4f spin−orbit coupling interaction. The energy separation between any two of those seven sub-states and the relative electric-dipole transition line strength from the $4f^7$ multiplet $^8S_{7/2}$ to any one can be taken from the calculation results given by ref 18 (SM details are given in the SI). Therefore, each of the bands A and B can be understood as a staircase structure of seven peaks with increasing intensity from low energy to high energy, and their maxima correspond to the vertical transition vibrational states of $|(4f^67F,s_d)^8F_{13/2};5d\Gamma_i\rangle$ (i = 1 and 2), respectively, as shown by the vertical bars in Figure 2a. Similarly, band C can be attributed to the transition from the lowest $4f^65d$ energy state $|(4f^67F,s_d)^8F_{1/2};5d\Gamma_1\rangle$ to the $4f^7$ multiplet $^8S_{7/2}$. Based on these assignments and the consideration of the electron−phonon coupling effect, the values of the Stokes shift parameter E_{shift} and the band barycenter parameters $E((4f^67F,s_d)^8F;5d\Gamma_i)$ (i = 1 and 2) for $Ca_{1.98}(Al_{1-x}Mg_x)(Al_{1-x}Si_{1+x})O_7$:0.02$Eu^{2+}$ can be extracted from the observed maxima of bands A−C and are collected in Table S4 (calculation details are provided in the SI). The calculated energy level schemes using the SM theory with the band barycenter parameter values $E((4f^67F,s_d)^8F;5d\Gamma_i)$ (i = 1 and 2) are plotted in Figure 2d. It is apparent from Figure 2d that the variation trend of the calculated $4f^65d$ energy level scheme versus x is in good agreement with the experimental results. The cases for x = 0 and 1 are shown by the solid and dashed vertical bars, respectively (corresponding to two 5d CF components), in Figure 2a for the sake of comparison. It can be deduced from Figure 2a that the trends for the two 5d CF components Γ_1 and Γ_2 are mutually exclusive as x increases.

The variation in fwhm versus x is similar to that of E_{shift} (Table S4). The configurational coordinate model, which has been successfully applied to Ce^{3+}-doped gadolinium gallium garnets,[19] has clearly confirmed a correlation between them. Therefore, using eq (10) of ref 19, one can easily calculate the Huang−Rhys factor S and the average energy of the local and effective phonon modes around Eu^{2+} ions $\hbar\hat{\omega}_{eff}$, which is recorded in Table S4. The decreasing trend with x indicates the electron−phonon coupling effect become weaker with increasing $[Mg^{2+}-Si^{4+}]$ content.

The relation between the structural evolution and photoluminescence properties of the studied materials should be clarified to improve the design ability of the optical properties of lanthanide-doped, isostructural, solid solution compounds. In melilite-type compounds, only the Ca^{2+} sites can be occupied by Eu^{2+}, and thus the 5d-4f emission band position will be determined by the local ligand environment of Eu^{2+} ions, i.e., the inner structure of the polyhedron $[(Ca/Eu)O_8]$. Here we employ the exchange charge model (ECM) to understand such a correlation since an essential feature of the model is that the 5d CF splitting calculations can be performed on real crystal structure data without a prior assumption of the symmetry of an impurity ion position.[20]

The 5d-4f emission energy $E(|(4f^67F,s_d)^8F_{1/2};5d\Gamma_1\rangle)$ of Eu^{2+} is found to be related to the difference between the lowest 5d CF component Γ_1 and the barycenter of the $5d^1$ configuration; the greater the difference, the greater the red-shift of the 5d-4f emission band position. The difference between any 5d CF component and the barycenter of the $5d^1$ configuration $E(5d\Gamma_i)$ (i = 1−5) can be evaluated by diagonalizing the parametrized 5d CF Hamiltonian matrix given by Reid.[21] All the calculated 5d CF parameters of Eu^{2+} in the solid solution $Ca_2(Al_{1-x}Mg_x)(Al_{1-x}Si_{1+x})O_7$:$Eu^{2+}$ (x = 0, 0.25, 0.5, 0.75, and 1) are collected in Table S5 and used in Reid's parametrized model. The absolute value of the energy difference between the lowest 5d CF component and the barycenter of the $5d^1$ configuration (i.e., $|E(5d\Gamma_1)|$) and the energy separation between the lowest two 5d CF components (i.e., $E(5d\Gamma_2) - E(5d\Gamma_1)$) is given in Table S6. The increasing trend of $|E(5d\Gamma_1)|$ with x supports the observed red-shift of the 5d-4f emission band position. Moreover, the increasing dependence of $E(5d\Gamma_2) - E(5d\Gamma_1)$ on x shows a good agreement with the experimental energy separation between the two 5d CF components (i.e, $E_{ex}(B) - E_{ex}(A)$), as shown in Figure 3a.

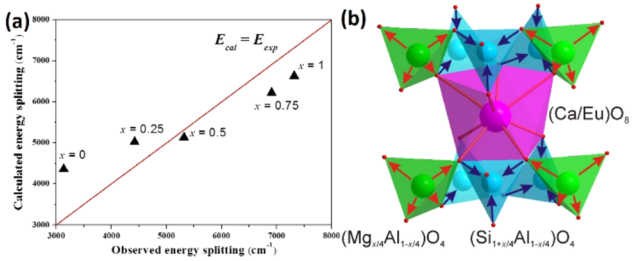

Figure 3. (a) Correlation of the calculated and experimental energy separation values between the lowest two 5d CF components as a function of x for the phosphors $Ca_{1.98}(Al_{1-x}Mg_x)(Al_{1-x}Si_{1+x})O_7$:0.02$Eu^{2+}$. (b) Structural distortion trend of the polyhedra $[(Ca/Eu)O_8]$: increasing of x leads to increasing $[(Mg/Al)O_4]$ polyhedra (red arrows) and decreasing $[(Si/Al)O_4]$ polyhedra (dark blue arrows).

The numerical simulation results can be more intuitively revealed from the local structure around Eu^{2+} dopants. The local structure after the replacement of two similar $[AlO_4]$ polyhedra by the larger $[MgO_4]$ and the smaller $[SiO_4]$ is shown in Figure 3b, and a typical distortion can be found owing to the breaking of the strict symmetry of the $[(Ca/Eu)O_8]$ polyhedra. To reveal the magnitude of the polyhedral distortion, we calculated the polyhedral distortion index (following the method reported by Baur)[22] as a function of x for the phosphors $Ca_{1.98}(Al_{1-x}Mg_x)(Al_{1-x}Si_{1+x})O_7$:0.02$Eu^{2+}$ (plotted in Figure S8). The calculated linear dependence increases, suggesting that the polyhedron becomes more distorted with increasing x. Such a distortion is thought to be responsible for the change of the 5d CF splitting, and similar results have been found in other systems.[23,24]

In summary, the chemical unit cosubstitution strategy has been corroborated both experimentally and computationally in the $Ca_2(Al_{1-x}Mg_x)(Al_{1-x}Si_{1+x})O_7$:$Eu^{2+}$ (x = 0−1) system, with $[Mg^{2+}-Si^{4+}]$ substituting for $[Al^{3+}-Al^{3+}]$. Structure computa-

DOI: 10.1021/jacs.5b08315
J. Am. Chem. Soc. 2015, 137, 12494−12497

tions and solid-state NMR spectra show the cosubstitution occurs solely on the 4-coordinate sites, and the lattice parameters obtained from the computations are in good agreement with those obtained from PXRD. The solid solution nature of the system enables tuning of the fluorescent properties. The red-shift of the 5d-4f emission peak of Eu^{2+} from 513 to 538 nm has been simulated by the crystal-field model and further confirmed by the polyhedral distortion model. The relationship between the electronic and structural properties has been supported by ECM calculations. The Stokes shift and the fwhm value for each Eu^{2+}-doped compound have been analyzed via the configurational coordinate model and trends obtained via quantitative description. Our results verify that the chemical unit cosubstitution will be a powerful strategy to discover new solid solution phosphors, and some controlled/tunable functional properties can be expected.

■ ASSOCIATED CONTENT

Supporting Information

The Supporting Information is available free of charge on the ACS Publications website at DOI: 10.1021/jacs.5b08315.

Experimental details, theoretical background, and calculation method, including Figures S1−S8 and Tables S1−S6, for $Ca_2(Al_{1-x}Mg_x)(Al_{1-x}Si_{1+x})O_7$ (x = 0, 0.25, 0.5, 0.75, and 1) compounds (PDF)

■ AUTHOR INFORMATION

Corresponding Authors

*xiazg@ustb.edu.cn
*cgma.ustc@gmail.com
*krp@northwestern.edu

Notes

The authors declare no competing financial interest.

■ ACKNOWLEDGMENTS

This work was supported by the National Natural Science Foundations of China (Grant Nos. 51572023 and 51272242), Natural Science Foundations of Beijing (2132050), the Program for New Century Excellent Talents in University of Ministry of Education of China (NCET-12-0950), Beijing Nova Program (Z131103000413047), and the Funds of the State Key Laboratory of Rare Earth Resource Utilization, Changchun Institute of Applied Chemistry, CAS (RERU2015022). C.M. acknowledges financial support from National Natural Science Foundation of China (Grant No. 11204393), Natural Science Foundation Project of Chongqing (Grant No. CSTC2014JCYJA50034), and National Training Programs of Innovation and Entrepreneurship for Undergraduates (Grant No. 201410617001). K.R. recognizes that this material is based upon work supported by the National Science Foundation Graduate Research Fellowship Program under Grant No. DGE-1324585.

■ REFERENCES

(1) Wang, G. F.; Peng, Q.; Li, Y. D. *Acc. Chem. Res.* **2011**, *44*, 322−332.
(2) Pust, P.; Weiler, V.; Hecht, C.; Tücks, A.; Wochnik, A. S.; Henß, A.; Wiechert, D.; Scheu, C.; Schmidt, P.; Schick, W. *Nat. Mater.* **2014**, *13*, 891−896.
(3) Chen, W. T.; Sheu, H. S.; Liu, R. S.; Attfield, J. P. *J. Am. Chem. Soc.* **2012**, *134*, 8022−8025.
(4) Park, W. B.; Singh, S. P.; Sohn, K. S. *J. Am. Chem. Soc.* **2014**, *136*, 2363−2373.
(5) Hirosaki, N.; Takeda, T.; Funahashi, S.; Xie, R. J. *Chem. Mater.* **2014**, *26*, 4280−4288.
(6) Ye, N.; Zeng, W. R.; Jiang, J.; Wu, B. C.; Chen, C. T.; Feng, B. H.; Zhang, X. L. *J. Opt. Soc. Am. B* **2000**, *17*, 764−768.
(7) Wang, C. C.; Chen, S. Y.; Yang, J. H.; Lang, L.; Xiang, H. J.; Gong, X. G.; Walsh, A.; Wei, S. H. *Chem. Mater.* **2014**, *26*, 3411−3417.
(8) Hoel, C. A.; Gallardo Amores, J. M.; Moran, E.; Angel Alario-Franco, M.; Gaillard, J.-F.; Poeppelmeier, K. R. *J. Am. Chem. Soc.* **2010**, *132*, 16479−16487.
(9) Swainson, I. P.; Dove, M. T.; Schmahl, W. W.; Putnis, A. *Phys. Chem. Miner.* **1992**, *19*, 185−195.
(10) Zhang, M.; Wang, J.; Ding, W. J.; Zhang, Q. H.; Su, Q. *Opt. Mater.* **2007**, *30*, 571−578.
(11) Zhang, Q.; Wang, J.; Zhang, M.; Su, Q. *Appl. Phys. B: Lasers Opt.* **2008**, *92*, 195−198.
(12) Denton, A. R.; Ashcroft, N. W. *Phys. Rev. A: At., Mol., Opt. Phys.* **1991**, *43*, 3161−3164.
(13) Shannon, R. D. *Acta Crystallogr., Sect. A: Cryst. Phys., Diffr., Theor. Gen. Crystallogr.* **1976**, *32*, 751−767.
(14) Mackenzie, K. J. D.; Smith, M. E. *Multinuclear solid-state NMR of inorganic materials*; Pergamon Press: Amsterdam, 2002.
(15) Dovesi, R.; Saunders, V. R.; Roetti, C.; Orlando, R.; Zicovich-Wilson, C. M.; Pascale, F.; Civalleri, B.; Doll, K.; Harrison, N. M.; Bush, I. J.; D'Arco, P.; Llunell, M. *CRYSTAL09 User's Manual*; University of Torino, 2009.
(16) Evarestov, R. A. *Quantum Chemistry of Solids*; Springer-Verlag: Heidelberg, 2007.
(17) Lv, W. Z.; Jia, Y. C.; Zhao, Q.; Jiao, M. M.; Shao, B. Q.; Lv, W.; You, H. P. *Adv. Opt. Mater.* **2014**, *2*, 183−188.
(18) Duan, C. K.; Reid, M. F. *J. Solid State Chem.* **2003**, *171*, 299−303.
(19) Przybylinska, H.; Ma, C.-G.; Brik, M. G.; Kaminska, A.; Szczepkowski, J.; Sybilski, P.; Wittlin, A.; Berkowski, M.; Jastrzebski, W.; Suchocki, A. *Phys. Rev. B: Condens. Matter Mater. Phys.* **2013**, *87*, 045114.
(20) Malkin, B. Z.; Kaplyanskii, A. A.; Macfarlane, R. M. *Spectroscopy of Solids Containing Rare Earth Ions*; North-Holland Publishing Co.: Amsterdam, 1987.
(21) Reid, M. F.; van Pieterson, L.; Wegh, R. T.; Meijerink, A. *Phys. Rev. B: Condens. Matter Mater. Phys.* **2000**, *62*, 14744−14749.
(22) Baur, W. H. *Acta Crystallogr., Sect. B: Struct. Crystallogr. Cryst. Chem.* **1974**, *30*, 1195−1215.
(23) Denault, K. A.; Brgoch, J.; Gaultois, M. W.; Mikhailovsky, A.; Petry, R.; Winkler, H.; DenBaars, S. P.; Seshadri, R. *Chem. Mater.* **2014**, *26*, 2275−2282.
(24) Miao, S. H.; Xia, Z. G.; Molokeev, M. S.; Chen, M. Y.; Zhang, J.; Liu, Q. L. *J. Mater. Chem. C* **2015**, *3*, 4616−4622.

DOI: 10.1021/jacs.5b08315
J. Am. Chem. Soc. 2015, 137, 12494−12497